Thermal X-ray Iron Line Emission from the Galactic Center Black Hole Sagittarius A*

Ya-Di Xu[1,2], Ramesh Narayan[2]

[1] *Physics Department, Shanghai Jiaotong University, Shanghai, 200030, China*

[2] *Harvard Smithsonian Center for Astrophysics, 60 Garden Street, Cambridge, MA 02138*
Email: ydxu@sjtu.edu.cn, narayan@cfa.harvard.edu

Eliot Quataert[3]

[3] *Astronomy Department, University of California, Berkeley, CA 94720*
Email: eliot@astron.berkeley.edu

Feng Yuan[4]

[4] *Department of Physics, Purdue University, 1396 Physics Building, West Lafayette, IN 47907-1396*
Email: fyuan@physics.purdue.edu

Frederick K. Baganoff[5]

[5] *Kavli Institute for Astrophysics and Space Research, Massachusetts Institute of Technology, Cambridge, MA 02139*
Email: fkb@space.mit.edu

ABSTRACT

We model thermal X-ray emission from the accreting supermassive black hole Sagittarius A* at the Galactic Center. For the region inside $1.''5$ of the center, we use a generalized radiatively inefficient accretion flow (RIAF) model, and for the region out to $10''$ we use published models of the ambient hot gas. We calculate the equivalent widths of Hydrogen-like and Helium-like emission lines of various elements, notably iron. We predict that a strong Helium-like iron line with an equivalent width ~ 1 keV should be emitted by both the external medium and the RIAF. The equivalent width in the external medium is sensitive to the metallicity Z of the gas as well as the mean temperature. For reasonable choices

of these parameters, the calculated results agree with Chandra's detection of an iron line with an equivalent width of 1.3 keV within $10''$. The emission from within $1.''5$ is not sensitive to the external temperature, but is sensitive to the density and, especially, temperature profile inside the Bondi radius. For the range of profiles we consider, we calculate the equivalent width of the iron line to be $\sim 0.6 - 1.5(Z/Z_\odot)$ keV, where $Z_\odot$ is the solar metallicity. We present a new Chandra spectrum of the quiescent emission within $1.''5$ of Sgr A*. The measured equivalent width of the iron line is 0.7 keV. Although this measurement has a large uncertainty, it is consistent with our predictions, provided the metallicity of the gas is approximately solar.

Subject headings: accretion, accretion disks—black hole physics —galaxies: nuclei—Galaxy: center—radiation mechanisms: thermal—X-rays: star

1. Introduction

Sagittarius A* (Sgr A*), the well known supermassive black hole of mass $M \approx 3.7 \times 10^6 M_\odot$ (Schödel et al. 2002; Ghez et al. 2005) at the center of the Galaxy, has attracted much attention for decades. Although the source is fairly bright in the radio band, it is overall quite dim, with a bolometric luminosity $L \approx 10^{36}$ ergs s$^{-1} \sim 10^{-8.5}L_{\rm Edd}$ and an X-ray luminosity $L_{\rm X} \approx 10^{33}$ ergs s$^{-1} \sim 10^{-11.5}L_{\rm Edd}$ in the 2-10 keV band (Baganoff et al. 2003).

X-ray emission from the region around Sgr A* was first observed by Einstein in the 0.5-4.5 keV band (Watson et al. 1981). Since then, many X-ray observations have been made by other satellites, e.g., ROSAT (Predehl & Trümper 1994; Predehl & Zinnecker 1996), ASCA (Koyama et al. 1996) and Beppo SAX (Sidoli et al. 1999). However all of these earlier observations gave only upper limits on the X-ray luminosity of Sgr A* because of poor spatial resolution. Recently, thanks to the excellent angular resolution and accurate astrometry of Chandra, Baganoff et al. (2001, 2003) succeeded for the first time to discriminate the emission of Sgr A* from that of surrounding point sources and hot plasma.

Chandra observations of the Galactic Center in 1999 and 2000 have revealed the following (Baganoff et al. 2001, 2003):

(1) The absorption-corrected quiescent luminosity of Sgr A* in the 2-10 keV band within $1.''5$ of the central source is $(1.8 - 5.4) \times 10^{33}$ ergs s^{-1}. The luminosity increases in the flare state by a factor of a few to a few tens.

(2) Fitting the observed spectrum in quiescence within $1.''5$ with an absorbed thermal

bremsstrahlung plus Gaussian-line model indicates a line centered at $6.5^{+0.4}_{-0.1}$ keV with an equivalent width of 2.2 keV. The temperature of the thermal plasma is 1.3-4.2 keV. We report in this paper an update on the properties of the line using newer data.

(3) The 2-10 keV luminosity of the diffuse emission within $10''$ is $(1.8-3.2)\times10^{34}$ ergs s^{-1}.

(4) Line emission at $6.5^{+0.1}_{-0.2}$ keV with equivalent width 1.3 keV is detected from the same region. The temperature of this plasma is fitted to be 1.3-2.0 keV.

The quiescent continuum spectrum of Sgr A* and the spectrum of the X-ray flares have been studied by a number of authors (e.g., Markoff et al. 2001; Yuan, Markoff & Falcke 2002; Liu & Melia 2001, 2002; Yuan, Quataert & Narayan 2003, 2004; Rockfeller et al. 2004; Nayakshin, Cuadra, & Sunyaev 2004; Goldston, Quataert, & Igumenshchev 2005). Yuan et al. (2003) present radiatively inefficient accretion flow (RIAF) models for Sgr A* and successfully explain the observed quiescent spectrum. Using nonthermal electrons, they are also able to account for the X-ray flares (Yuan, Quataert & Narayan 2003) and IR variability (Yuan, Quataert & Narayan 2004).

The following consensus has emerged from these modeling efforts. The radio, sub-millimeter and infrared emission all come from close to the black hole, say from a few R_S (sub-mm, infrared) to $100R_S$ (radio), where $R_S = 2GM/c^2$ is the Schwarzschild radius of the black hole. The infrared and X-ray flare emission are also from small radii (few R_S). In contrast, the quiescent X-ray emission is from large radii, near the Bondi capture radius $R_{\rm B} \simeq GM/c_{\rm s}^2 \simeq 10^5 R_S \simeq 1''$, where c_s is the sound speed of the ambient gas in the external medium. Therefore, depending on one's interests, one must focus on different regions of the spectrum. To study the mean features of the flow near the black hole, the radio and sub-mm emission are most useful. To understand transient phenomena near the black hole, one must focus on the infrared and X-ray flares. And if, as in the present paper, one wishes to study the transition region of the flow where the external gas is captured by the black hole and begins to fall in, the quiescent X-ray emission is the radiation of choice.

Quataert (2002) has presented model X-ray spectra for the hot ambient gas around Sgr A*. He models the transition region where the gas flows in from the external medium, and calculates the thermal bremsstrahlung emission. His model explains the soft X-ray spectrum, the relatively constant quiescent flux, and the spatially resolved nature of the source. In later work, Quataert (2004) describes detailed dynamical gas models on scales $\sim 0.01-1$ pc. These models incorporate both accretion onto the black hole and a wind from the central star cluster. The models show that only a few percent of the gas supplied by stellar winds in the central parsec is gravitationally captured by Sgr A* (see Coker & Melia 1997; Cuadra et al. 2005a,b for 3D simulations), implying an accretion rate at the Bondi

radius of $\sim$a few $\times 10^{-5}$ $M_\odot \mathrm{yr}^{-1}$; the remaining gas, $\sim 10^{-3}$ $M_\odot \mathrm{yr}^{-1}$, is thermally driven out of the central star cluster in a wind. The emission from the outflowing hot gas accounts for the observed level of diffuse X-ray emission in the central $10''$ of the Galactic Center.

While most of the work so far has focused on the continuum spectrum of Sgr A*, the emission lines also provide important constraints. Prior to the Chandra observations, Narayan & Raymond (1999) predicted, using advection dominated accretion flow (ADAF) models, that thermal X-ray line emission should be seen from Sgr A*. In the present work, we use Quataert's (2002, 2004) models of the transition region to explore the thermal X-ray line emission from Sgr A* and from the diffuse gas surrounding the black hole (outside the Bondi radius). To carry out these calculations, we need to model the gas interior to the Bondi radius, down to about $\sim 0.1 R_B$. For convenience, we use the RIAF model of Yuan et al. (2003) as our default model. However, we also allow the density and temperature profiles some freedom, in order to assess how the observations of line emission can constrain the dynamics down to $\sim 0.1 R_B$. In §2, we describe the details of our dynamical models. In §3, we describe the calculations of line emission and present the results. We conclude in §4 with a comparison of the model with current observations and discuss some implications of this work.

2. Models

2.1. Models of the Ambient Medium

Thanks to the high angular resolution of Chandra, it is possible to clearly distinguish between emission from the accretion flow around Sgr A* and that produced by the surrounding ambient plasma. This means that we can, in principle, constrain the properties of both components. We make use of five different models from Quataert (2002, 2004) to describe the ambient hot gas.

Quataert (2002) obtains temperature and density profiles (see his Fig. 1) based on two different prescriptions. The first model assumes that the ambient medium is stratified with $\rho \propto R^{-1}$ for $R \gtrsim R_\mathrm{B}$ (the physics responsible for the stratification was not important in these calculations, which were actually based on cooling flow models in clusters of galaxies; see Quataert & Narayan 2000). We refer to this as model A. The second model is the original Bondi flow in which the external medium is taken to be uniform. We refer to this as model B. For a given system, the relative contribution of the accretion flow ($R \lesssim R_\mathrm{B}$) and the ambient medium ($R \gtrsim R_\mathrm{B}$) to the observed thermal bremsstrahlung emission depends on the beam size of the telescope (R_beam). For $R_\mathrm{beam} \gg R_\mathrm{B}$, the ambient medium dominates the

observed emission, while for $R_{\rm beam} \ll R_{\rm B}$, the accretion flow does. Chandra has $R_{\rm beam} \approx R_{\rm B}$ for the Galactic Center, and so Quataert proposes that the quiescent emission from Sgr A* arises from gas at $\sim R_{\rm B}$, i.e., from the "transition region" between the external medium and the accretion flow. To reproduce the observed luminosity of Sgr A* in the quiescent state, gas densities at $1.''5$ (corresponding to $R \approx 10^{5.2} R_S$) and $10''$ (corresponding to $R \approx 10^6 R_S$) should be ≈ 100 cm^{-3} and ≈ 20 cm^{-3}, suggesting that a stratified external medium (model A) is more appropriate than a uniform medium (model B).

Quataert (2004) has described more elaborate models of the hot gas in which he incorporates stellar winds as a source of mass and energy in the equations of hydrodynamics. Noting that the observed mass-losing stars are located several arcseconds from the black hole, Quataert models the stellar mass loss per unit volume as $q(r) \propto r^{-\eta}$ for $r \in [10^{5.3}, 10^6]$, where $r = R/R_S$ is the dimensionless radius, and obtains the local mass injection rate as $d\dot{M}_{\rm w}/d{\rm ln}r \propto r^{-\eta+3}$. Taking a wind velocity $v_{\rm w} \approx 1000$ km s^{-1} and a total mass injection rate $\dot{M}_{\rm w} = \int 4\pi r^2 q(r) dr \approx 10^{-3} M_\odot {\rm yr}^{-1}$, he explores three cases, $\eta = 2$, 3, and 0, which we refer to as models C, D, and E, respectively. The solutions show that a few percent of the mass supplied by the stellar winds, $\sim$few$\times 10^{-5} M_\odot {\rm yr}^{-1}$, is gravitationally captured by the BH while the majority of the gas, $\sim 10^{-3} M_\odot {\rm yr}^{-1}$, is driven out of the central parsec. The models account for the level of diffuse X-ray emission observed in the central $10''$ of the Galactic Center, and predict an electron density of $\sim$20-30 cm^{-3} at $\sim 10''$ radius, consistent with Chandra observations.

2.2. Models of the Dynamics Inside R_B

In the present work, we make use of models A-E for radii outside the Bondi radius. For $R \lesssim R_B$, we allow the density and temperature profiles to be of the form

$$n_e(r) \propto r^{-3/2+s} \equiv r^{-p}, \tag{1}$$

$$T_e(r) \propto r^{-q}. \tag{2}$$

The motivation for allowing this freedom in the two profiles at small radii is that the dynamics at radii $\lesssim R_B$ depends on uncertain physics, e.g., the radius at which the flow circularizes, the importance of thermal conduction (e.g., Gruzinov 1998), and the rate of electron heating. We wish to explore the extent to which observations of line emission can constrain the dynamics of the flow inside R_B, and thus it is necessary to consider a variety of models for the density and temperature profiles.

We take the density and temperature profiles from the Yuan et al. (2003) RIAF model as our baseline model, since this model provides a good description of the observed spectrum

from Sgr A*. The Yuan et al. model corresponds to $p \approx 1.13$ and $q \approx 1$. We also consider variations about this model, namely density profiles with $p = 0.5, 0.75, 1.25$, and 1.5 and temperature profiles with $q = 0.25, 0.5$, and 0.75. For simplicity, we refer to all of these models as RIAFs, and we identify the region of the flow inside the Bondi radius as the RIAF.

In the calculations, we choose one of models A-E from Quataert (2002, 2004) to describe the external medium down to $R = 10^5 R_{\rm S} \approx R_B$. Inside this radius, we smoothly match on to the selected density and temperature profiles described above.

To compare our calculations with observations of the temperature of the ambient thermal plasma, we also allow for small variations in the electron temperature of the models at large radii. Observations indicate that this temperature is in the range 1.2-2.0 keV (Baganoff et al. 2003), so we consider a series of models with $kT_e(r = 10^{5.5})$ in this range. To do so, we scale the entire temperature of Quataert's (2002, 2004) models to the desired $kT_e(r = 10^{5.5})$. (We fix the temperature at $\log r = 5.5$, which is "mid-way" between the outermost radius we consider, $\log r = 6 = 10''$, and the radius where the external medium transitions to the RIAF, $\log r = 5$.) We then study the variation of the equivalent width of the He-like iron line from the RIAF and the ambient medium, respectively. Strictly speaking, this procedure is not fully consistent since variations in $kT_e(r = 10^{5.5})$ would also lead to variations in R_B and the dynamics at smaller radii, but for the narrow range of external temperatures considered here, such variations are small compared to the significant changes in equivalent width caused by different models of the ambient medium and different density and temperature profiles at $R \lesssim R_B$.

The model density and electron temperature profiles corresponding to $kT_e(r = 10^{5.5}) = 1.5$ keV are displayed in Figures 1 and 2 for the case in which we use the Yuan et al. RIAF model inside R_B.

3. Calculations and Results

3.1. Calculations of Line Equivalent Widths

Using the models of the RIAF and the hot ambient medium described in the previous section, we have computed the thermal X-ray line emission from Sgr A* within $1.''5$ of the center and within $10''$. The equivalent width of an emission line is defined as

$$\mathrm{EW}_{\rm line} = L_{\rm line}/L_\nu(\nu_{\rm line}), \tag{3}$$

where L_{line} is the total luminosity of the emission line, and $L_\nu(\nu_{\text{line}})$ is the spectral luminosity of the continuum at the energy of the line $h\nu_{\text{line}}$.

To obtain the spectral luminosity and the total line luminosity L_{line}, we integrate over the luminosities contributed by different shells of the accretion flow and the ambient hot gas,

$$L_{\text{line}} = \int_{r_{\text{min}}}^{r_{\text{max}}} n_e^2 \cdot \epsilon_{\text{line}} \cdot 4\pi r H \cdot dr \cdot R_{\text{S}}^2, \tag{4}$$

$$L_\nu(\nu_{\text{line}}) = \int_{r_{\text{min}}}^{r_{\text{max}}} n_e^2 \cdot \epsilon_\nu(\nu_{\text{line}}) \cdot 4\pi r H \cdot dr \cdot R_{\text{S}}^2, \tag{5}$$

where n_e is the electron density at dimensionless radius $r = R/R_{\text{S}}$; $r_{\text{min}} \equiv R_{\text{min}}/R_{\text{S}}$ and $r_{\text{max}} \equiv R_{\text{max}}/R_{\text{S}}$ are the inner and outer radii of the line emission region under study. We adopt $r_{\text{max}} \approx 10^{5.2}$ and $r_{\text{max}} \approx 10^6$, which correspond to $1.''5$ (the RIAF) and $10''$ (the external medium) at the distance of Sgr A*. Most of the line emission of interest is produced at radii between $\sim 0.1 R_B \sim 10^4 R_{\text{S}}$ and R_{max} so the exact value of R_{min} is not that important.

We calculate the vertical half thickness H of the accretion flow self-consistently in the RIAF model and set $H = r R_{\text{s}}$ for the spherically symmetric external medium ($r \gtrsim 10^{5.2}$). The quantities ϵ_{line} and $\epsilon_\nu(\nu_{\text{line}})$ are the line and continuum emissivities at a certain radius, which are functions of the local temperature.

Given the electron temperature from the model, we use the standard software package Astrophysical Plasma Emission Code (APEC) (Smith et al., 2001) to calculate the emissivity of the chosen line. We assume a solar abundance and ionization equilibrium in the calculations. The APEC code includes collisional excitation, recombination to excited levels and dielectronic satellite lines. It ignores photoionization, which is a few percent effect at most (Narayan & Raymond 1999). We employ the APEC code also to calculate the spectral continuum luminosity $L_\nu(\nu_{\text{line}})$ from bremsstrahlung, radiative recombination and two photon emission from the region in which the electron temperature is lower than 10^9K, and use the prescription given in Narayan & Yi (1995) to calculate the bremsstrahlung emission from the inner hot region ($T_e \geq 10^9$K).

While our primary interest is H-like and He-like iron lines, we also compute H-like and He-like line equivalent widths of some other elements, such as Si, S, Ar, Ca, and Ni. In view of the poor energy resolution of the observations, we combine the lines in bins of 100 eV width. We ignore Doppler and thermal broadening of lines, which are below the energy resolution of Chandra.

The equivalent widths of lines from the RIAF ($\lesssim 1.''5$) and the ambient medium ($\lesssim 10''$) around Sgr A* are represented as EW_1 and EW_2, respectively. They are directly proportional

to the metallicity Z of the accreting gas,

$$\mathrm{EW}_{1,2}(Z) = \frac{Z}{Z_\odot}\mathrm{EW}_{1,2}(Z_\odot), \tag{6}$$

where $Z_\odot$ is the solar metallicity. All the equivalent width results presented in this paper correspondent to $\mathrm{EW}_{1,2}(Z_\odot)$, i.e., for solar metallicity. They can be scaled to other metallicities using equation (5).

3.2. Results

The equivalent widths of some relatively strong H-like and He-like lines of high-Z ions are listed in Tables 1 and 2. The calculations are for the Yuan et al. (2003) RIAF model matched to each of the five external models A–E. Table 1 gives $\mathrm{EW}_1(Z_\odot)$ corresponding to the radiation from within $1.''5$ of Sgr A*, while Table 2 shows the corresponding line widths $\mathrm{EW}_2(Z_\odot)$ from within $10''$ around Sgr A*. For the RIAF (EW_1), note that the He-like Fe XXV line is strong, with the H-like Fe XXVI line being second in importance . For the external medium (EW_2), however, the electron temperature of the gas is too low to produce H-like iron emission; hence there is no entry for this line.

Figures 3 and 4 show the variation of the EW of He-like iron line from the RIAF (EW_1) and the ambient medium (EW_2) as a function of the external electron temperature $kT_e(r = 10^{5.5})$. Stars, crosses, squares, circles, and triangles correspond to the five models of the external medium, A, B, C, D, and E, respectively. Figure 3 shows that EW_1 from the accretion flow is virtually independent of the external temperature, giving a value $\sim 0.6 - 0.7$ keV for solar metallicity. In contrast, Figure 4 shows that EW_2 from the external medium varies significantly with $kT_e(r = 10^{5.5})$, going from 0.5 keV to 1.5 keV as this temperature is varied. By combining the line and continuum data from this region, one should in principle be able to solve for both $kT_e(r = 10^{5.5})$ and metallicity Z. Once we have Z, we should then be able to compare the expected equivalent width from the RIAF (EW_1) with observations.

Changing the density law index p of the self-similar RIAF solution from 0.5 (very strong reduction of $\dot{M}_{BH}$ relative to $\dot{M}_{out}$) to 1.5 ($\dot{M}_{BH} = \dot{M}_{out}$), keeping Yuan et al.'s RIAF model for the temperature profile, and using model A for the external medium, we obtain different estimates of EW_1. The results are displayed in Figure 5(a). Larger values of p like 1.25 and 1.5 are inconsistent with constraints on the density near the black hole as obtained from radio polarization data (Bower et al. 2003). The remaining three models give EW_1 values in the range 0.7-1.0 keV, i.e., not very different from the baseline model.

We also consider deviations in the temperature profile of the RIAF from Yuan et al's

model, which has $T_e \sim r^{-1}$. The temperature is unlikely to increase more steeply with decreasing r since r^{-1} corresponds to the virial slope, but it could be shallower. We therefore try temperature profiles $T_e \propto r^{-3/4}$, $r^{-1/2}$, $r^{-1/4}$, retaining Yuan et al's density profile. The results are compared with the original results of "RIAF+ model A" in Figure 5(b). We see that EW_1 increases from 0.7 keV to nearly 1.5 keV. Thus, EW_1 is fairly sensitive to the temperature profile, and so the observations can be used to constrain the radial variation of the electron temperature.

4.   Discussion

In this paper we have analyzed thermal X-ray line emission from the Galactic Center. We consider the outer regions of the accretion flow onto the massive black hole Sagittarius A* as well as the external gas surrounding the black hole. For the former we employ Yuan et al.'s (2003) radiatively inefficient accretion flow (RIAF) model modified in various ways through the parameters p and q in equations (1) and (2), and for the latter we use five different models (A–E) from Quataert (2002, 2004). The models are matched at a radius of $10^5 R_S \approx R_B$ by shifting their temperature and/or density profiles by small amounts. The emission observed from within 1."5 of Sgr A* (radii $\lesssim 10^{5.2} R_S$) is interpreted as coming from the accretion flow (the RIAF[1]), and the emission between 1."5 and 10" is viewed as coming from the external medium. We compute the equivalent widths of hydrogen-like and helium-like lines of various metals in the two zones.

Our calculations show that the X-ray emission from the RIAF should have a strong He-like thermal iron line at an energy of 6.70 keV. For our baseline model (the Yuan et al. RIAF), the equivalent width $EW_1 \sim 0.6 - 0.7(Z/Z_\odot)$ keV, where Z is the metallicity of the accreting gas and $Z_\odot$ refers to solar metallicity. We find that EW_1 is quite insensitive to the details of the external gas model to which the RIAF is matched (see Fig. 3). When we allow for variations in the density profile within the RIAF by adjusting the parameter p, we obtain $EW_1 \sim 0.6 - 1.0(Z/Z_\odot)$ keV (Fig. 5a), which is still a fairly narrow range. On the other hand, variations in the temperature profile (q varied over the range 0.25 to 1) cause a larger range, $EW_1 \sim 0.7 - 1.5(Z/Z_\odot)$ keV (Fig. 5b). Thus, with an independent estimate of Z, it should be possible to test the dynamics of the flow inside R_B and, in particular, constrain the electron temperature profile via the parameter q.

Figure 6 shows the integrated quiescent spectrum of Sgr A* obtained by combining the

---

[1]Technically, the RIAF is present only inside the Bondi radius at $\sim 10^5$. However, the best spatial resolution possible with *Chandra* is $r \sim 10^{5.2}$, so we treat the entire region inside this radius as the RIAF.

twelve Chandra pointings performed during the period 1999 September 21 through 2002 June 4 (see Table 2 in Muno et al. 2003). The total effective exposure is 590 ks. The source spectrum was extracted from a circular region with radius $1.''5$ centered on the radio position of Sgr A* (Reid et al. 1999), and the background spectrum was extracted from an annulus with inner and outer radii of $2''$ and $10''$, respectively. Discrete sources within the background annulus were excluded as described by Baganoff et al. (2003).

Using only the spectrum from about 3 keV to 10 keV, we fit the data with an absorbed, thermal bremsstrahlung plus Gaussian-line model, including a correction for the effects of dust scattering as described by Baganoff et al. (2001). The best-fit model ($\chi^2/\mathrm{dof} = 111.1/111$) is shown in Figure 6. The parameter values are $N_\mathrm{H} = 9.34^{+0.85}_{-0.82} \times 10^{22}$ cm^{-2}, $kT_\mathrm{e} = 3.24^{+0.43}_{-0.31}$ keV, $E_\mathrm{Fe} = 6.61^{+0.05}_{-0.05}$ keV, and $\sigma_\mathrm{Fe} = 94.5^{+63.5}_{-47.2}$ eV, where N_H is the absorption column density, kT_e is the electron temperature of the emitting plasma, and E_Fe and σ_Fe are, respectively, the energy and standard deviation of the emission line. The quoted uncertainties are the 90% confidence intervals for one interesting parameter.

The emission line has an equivalent width of 706 eV, with a 90% confidence lower limit of 314 eV. Unfortunately, the steep fall-off in the effective area of the Chandra mirrors above 7 keV prevents the fitting routine from determining a reliable upper-limit on the equivalent width. Additional observations will be required to obtain a sufficient signal above 7 keV to measure the full properties of this line. A recent study by Najarro et al. (2004) of the NIR spectra of five massive stars in the nearby Arches Cluster indicates that the stellar metallicity in the cluster is about solar. Sgr A* is believed to be accreting material from the winds of similar massive, windy stars in the central parsec cluster, so the results of Najarro et al. (2004) suggest that the plasma accreting onto Sgr A* may have solar abundances as well. The agreement found between the best-fit equivalent width of the observed spectrum and the predictions of our models are then striking.

As expected, the spectral width of the line is unresolved by Chandra/ACIS. The best-fit line energy (6.61 keV) is centered below that of He-like Fe (6.70 keV), and the 90% upper limit (6.66 keV) falls just shy of it. The dielectronic satellites (DES) may be responsible for this tiny redshift. Oelgotz & Pradhan (2001) show that the dielectronic satellites, which appear redward of w line at 6.70 keV and prominently exist around 6.65 keV at low temperature, dominate X-ray spectral formation in the 6.7 keV Kα complex of Fe XXV at temperature below that of maximum abundance in collisional ionization equilibrium T_m ($\approx 3 \times 10^7$ for Fe XXV) and make the He-like iron Kα lines redshifted from 6.7 keV. After more detailed calculation, we find that, for all He-like iron lines centered between 6.0 keV and 7.0 keV, the luminosity-weighted mean energy is near $6.665 \sim 6.680$ keV for different models used in this paper.

In addition to a strong He-like iron line, the RIAF model predicts a H-like iron line at 6.97 keV. However, the equivalent width of this is only a fifth of the He-like line. The model also predicts lines from a number of other elements, but with even smaller equivalent widths. These lines are presently not useful, but may provide useful diagnostics of the accretion flow in the future.

In contrast to the emission from within R_B, the line emission from the external medium shows large variations with model parameters. The equivalent width EW_2 of the He-like iron line varies significantly as the temperature $kT_e(r = 10^{5.5})$ of the external gas is varied (see Fig. 4). There is also a modest variation between the five models from Quataert (2002, 2004) that we used for the gas. Overall, we find values of EW_2 in the range $0.4 - 1.6(Z/Z_\odot)$ keV, which corresponds to a factor of four uncertainty.

The very different sensitivities of EW_1 and EW_2 to shifts in the overall electron temperature profile, as parameterized by $kT_e(r = 10^{5.5})$ — compare Figures 3 and 4 — may be understood in terms of the different temperature profiles of the two regions. Figure 7 shows the dependence of the line and continuum emissivities as a function of temperature. In the RIAF, the electron temperature is larger than 2 keV and increases with decreasing radius (Fig. 2), and the iron line and continuum emission come mainly from gas at temperatures in the range $\sim (2-\text{several})$ keV. When the temperature profile rises up, the most efficient emission region moves to larger radii and the radiating volume becomes larger. However, the line and continuum change by roughly similar amounts, thus maintaining EW_1 almost unchanged (Fig. 7). In contrast, the electron temperature of the external gas is lower than 2 keV and varies much less with radius. Here, both the line and continuum emission increase sharply with increasing temperature, and since the line varies much more than the continuum, the equivalent width changes significantly (Fig. 7).

In our model, we have included bound-bound, bound-free and free-free emission from the hot gas, but we have not considered Compton scattering. The latter is produced in a RIAF by the ultra-hot gas in the innermost region near the black hole. However, at the very low mass accretion rate present in Sgr A*, and especially for the flat density profile ($p \sim 1$ or less) required by the observations, Comptonization is quite unimportant (see Yuan et al. 2003). For the two lowest sets of models in Figure 5(a) (open dots and crosses), Comptonization could be important (it would cause EW_1 to decrease). However, those models are ruled out for other reasons, and therefore Comptonization is not a concern for this work.

The assumption of ionization equilibrium in our calculations needs further study, especially for the gas outside of the Bondi radius. Baganoff et al. (2003) observed a line in this region at $6.5^{+0.1}_{-0.2}$ keV, which is intermediate in energy between He-like and lower ionization state lines of iron. They suggested that the external plasma is perhaps in a state of

nonionization equilibrium (NIE). If the heating rate in the plasma is larger than the thermalization or ionization rates, then a NIE plasma will result with strong emission lines from low-ionization state ions.

The gas in the vicinity of Sgr A* has probably been compressed by the passage of a shock wave associated with Sgr A East, which is believed to be a supernova remnant (SNR). Alternatively, the gas may have been influenced by multiple SNRs or by an extremely energetic explosion resulting from the tidal disruption of a star by the central black hole (see Maeda et al. 2002 and references there in). More plausibly, the gas, which is most likely supplied by nearby stars, is shocked in colliding winds (Quataert 2004). Plasmas in SNRs are generally not in ionization equilibrium, so any of the above scenarios will lead naturally to a NIE state for the gas. Modelling the thermal line emission from NIE plasmas is challenging, but such a study would be worthwhile for the gas surrounding Sgr A* if more detailed observations become available.

REFERENCES

Agol, E. 2000, ApJ, 538, L121

Aitken, D. K. et al. 2000, ApJ, 534, L173

Baganoff, F. K., et al. 2001, Nature, 413, 45

Baganoff, F. K., et al. 2003, ApJ, 591, 891

Blandford, R. D., & Begelman, M. C. 1999, MNRAS, 303, L1

Bower, G. C., Wright, M. C. H., Falcke, H., & Backer, D. C. 2003, ApJ, 588, 331

Coker, R.F., & Melia, F. 1997, ApJ, 488, L149

Cuadra, J., Nayakshin, S., Springel V. & Matteo, T. D. 2005, MNRAS, 360, L55

Cuadra, J., Nayakshin, S., Springel V. & Matteo, T. D. 2005, astro-ph/0505382

Ghez, A. M., Salim, S., Hornstein, S. D., Tanner, A., Lu, J. R., Morris, M., Becklin, E. E., & Duchêne, G. 2005, ApJ, 620, 744

Goldston, J. E., Quataert, E. & Igumenshchev, I. V. 2005, ApJ, 621, 785

Gruzinov A. 1998, astro-ph/9809265

Hawley, J. F., & Balbus, S. A. 2002, ApJ, 573, 738

Igumenshchev, I. V., & Abramowicz M. A. 1999, MNRAS, 303,309

Igumenshchev, I. V., Abramowicz, M. A., & Narayan R. 2000, ApJ, 537, L27

Igumenshchev, I. V., Narayan, R., & Abramowicz M. A. 2003, ApJ, 592, 1042

Koyama, K., Maeda, Y., Sonobe, T., Takeshima T., Tanaka, Y., & Yamauchi, S. 1996, PASJ, 48, 249

Liu, S. & Melia, F. 2001, APJ 561, L77

Liu, S. & Melia, F. 2002, APJ 566, L77

Maeda, Y., et al. 2002, ApJ, 570, 671

Mahadevan, R. 1998, Nature, 394, 651

Markoff, S., Falcke, H., Yuan, F., Biermann, P. L. 2001, A&A, 379, L13

Muno, M. P., et al. 2003, ApJ, 589, 225

Najarro, F., Figer, D. F., Hillier, D. J., & Kudritzki, R. P. 2004, ApJ, 611, L105

Narayan, R. 2002, in Lighthouse of the Universe, ed. M. Gilfanov et al. (Berlin:Springer), 405

Narayan R., Igumenshchev, I. V., & Abramowicz, M. A. 2000, ApJ, 539, 798

Narayan, R., Mahadevan, R., Grindlay, J. E., Popham, R., & Gammie, C. 1998, ApJ, 492, 554

Narayan, R., & Raymond, J. 1999, ApJ, 515, L69

Narayan, R., Yi, I., & Mahadevan, R. 1995, Nature, 374, 623

Narayan, R. & Yi, I. 1995, ApJ, 452, 710

Nayakshin, S., Cuadra, J., & Sunyaev, R. 2004, A&A, 413, 173

Oelgoetz J. & Pradhan A. K. 2001, MNRAS, 327, L42

Predehl, P., & Trümper, J. 1994, A&A, 290, L29

Predehl, P., & Zinnecker, H. 1996, in ASP Conf. Ser. 102, The Galactic Center, ed. R. Gredel
        (San Francisco:ASP), 415

Quataert, E. 2002, ApJ, 575, 855

Quataert, E. 2004, ApJ, 613, 322

Quataert, E., & Gruzinov, A. 2000a, ApJ, 539, 809

Quataert, E., & Gruzinov, A. 2000b, ApJ, 545, 842

Quataert, E., & Narayan, R. 1999, ApJ, 520, 298

Quataert, E., & Narayan, R. 2000, ApJ, 528, 236

Quataert, E., Narayan, R., & Reid, M.J. 1999, ApJ, 517, 101

Reid, M. J., Readhead, A. C. S., Vermeulen, R. C., & Treuhaft, R. N. 1999, ApJ, 524, 816

Rockfeller, G., Fryer, C. L., Melia, F., & Warren, M. S. 2004, ApJ, 604, 662

Schödel, R., et al. 2002, Nature, 419, 694

Sidoli, L., Mereghetti, S., Israel, G., L., Chiappetti, L., Treves, A., & Orlandini, M. 1999,
        ApJ, 525, 215

Smith, R. K., Brickhouse, N. S., Liedahl, D. A., & Raymond, J. C. 2001, ApJ, 556, L91

Stone, J. M., & Pringle, J. E. 2001, MNRAS, 322, 461

Stone, J., Pringle, J. & Begelman, M. 1999, MNRAS, 310, 1002

Yuan, F., Markoff, S., & Falcke, H. 2002, A&A, 383, 854

Yuan, F., Quataert, E., & Narayan, R. 2003, ApJ, 598, 301

Yuan, F., Quataert, E., & Narayan, R. 2004, ApJ, 606, 894

Watson, M. G., Willingale, R., Grindlay, T. E., & Hertz, P. 1981, ApJ, 250, 142

Table 1.   Equivalent widths $EW_1(Z_\odot)$ in units of eV of X-ray lines from the RIAF $(R < 10^{5.2}R_S)$

Line & E_C	(keV)	A	B	C	D	E
Si XIII	1.866	13	18	22	23	23
Si XIV	2.007	55	64	69	70	70
S XV	2.462	31	42	49	50	50
S XVI	2.624	51	57	57	58	58
Ar XVII	3.141	21	25	27	27	27
Ar XVIII	3.325	14	14	13	13	13
Ca XIX	3.908	23	26	25	26	26
Fe XXIV	6.663	26	26	25	26	26
Fe XXV	6.700	702	712	675	675	680
Fe XXVI	6.970	142	143	151	151	150
Fe XXV	7.800	24	25	23	23	24
Ni XXVII	7.813	23	23	22	21	21

Note. — These lines are from the accretion flow inside 1."5 of Sgr A* for five models A-E, with $kT_e(r = 10^{5.5}) = 1.5$ keV .
Model A: RIAF + stratified density hot gas model
Model B: RIAF + uniform density hot gas model
Model C: RIAF + "$\eta = 2$" dynamical hot gas model
Model D: RIAF + "$\eta = 3$" dynamical hot gas model
Model E: RIAF + "$\eta = 0$" dynamical hot gas model

Table 2.   Equivalent widths $EW_2(Z_\odot)$ in units of eV of X-ray lines from the external medium $(10^{5.2}R_S < R < 10^6 R_S)$

Line & E_C	(keV)	A	B	C	D	E
Si XIII	1.866	159	141	95	102	102
Si XIV	2.007	165	167	152	155	156
S XV	2.462	213	211	172	178	179
S XVI	2.624	75	79	91	90	90
Ar XVII	3.141	75	77	71	72	73
Ar XVII	3.325	7	7	10	10	10
Ca XIX	3.908	61	62	61	61	61
Fe XXIV	6.663	203	230	219	223	227
Fe XXV	6.700	1007	937	1208	1187	1173
Fe XXVI	6.970	-	-	-	-	-
Fe XXV	7.800	87	79	101	100	98
Ni XXVII	7.813	17	14	16	15	15

Note. — These lines are from within 10" of Sgr A* for five models A-E, with $kT_e(r = 10^{5.5}) = 1.5$ keV.
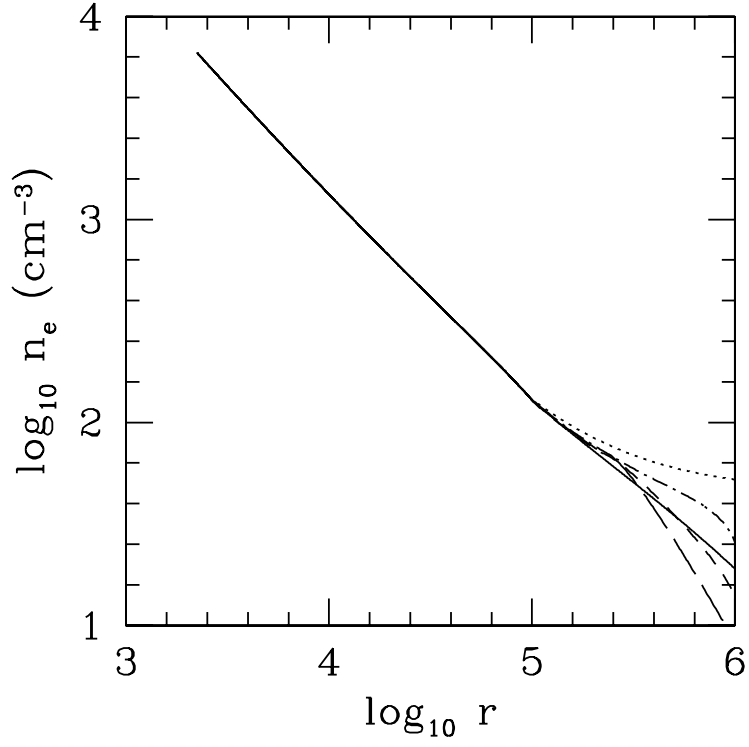
Fig. 1.— Model electron density profile of the baseline model. For $r \equiv R/R_S < 10^5$ the profile is from Yuan et al. (2003), and for $r > 10^5$ it corresponds to one of five models from Quataert (2002, 2004). Solid, dotted, short dashed, long dashed, and dot-short dashed lines correspond to models A, B, C, D, E, respectively. The profiles have been adjusted so as to match smoothly at $r = 10^5$. (See text for details.)
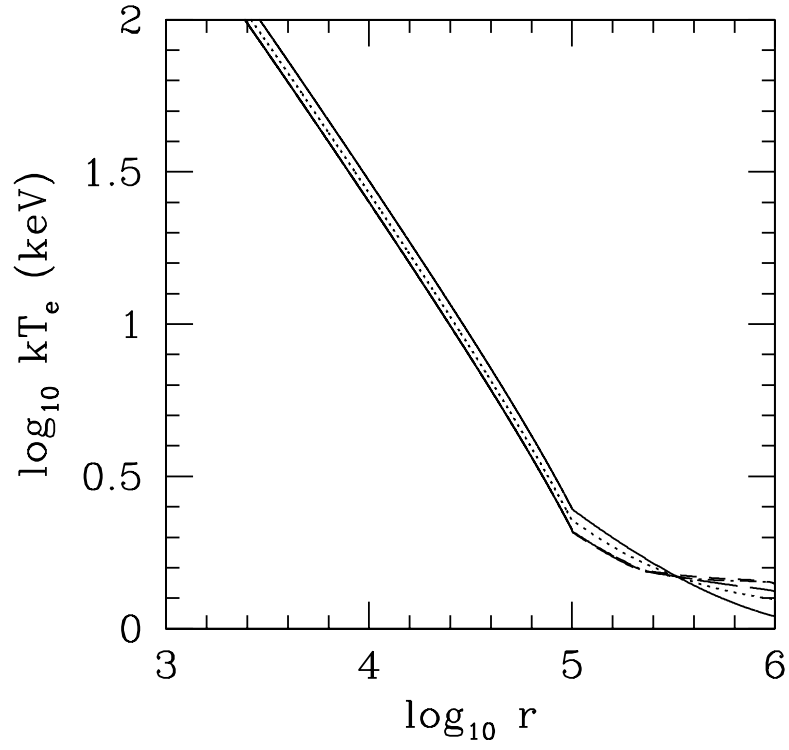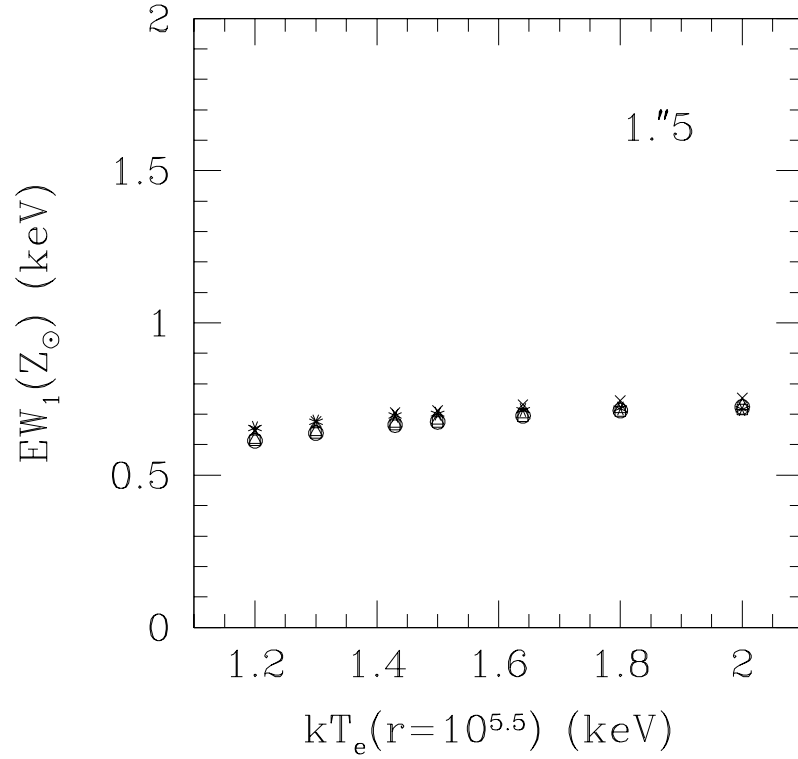
Fig. 2.— Electron temperature profiles for the same models as in Fig. 1. All five models have been adjusted to have $kT_e(r = 10^{5.5}) = 1.5$ keV. Solid, dotted, short dashed, long dashed, and dot-short dashed lines correspond to models A, B, C, D, E, respectively.

Fig. 3.— Variation of the equivalent width EW_1 of He-like iron line emission from the baseline model of the RIAF ($\lesssim 1.''5$, $r < 10^{5.2}$) as a function of the assumed external electron temperature $kT_e(r = 10^{5.5})$. Stars, crosses, squares, circles, and triangles correspond to the results for models A, B, C, D, E, respectively. Note that EW_1 is practically independent of $kT_e(r = 10^{5.5})$ and is nearly the same for all five models.
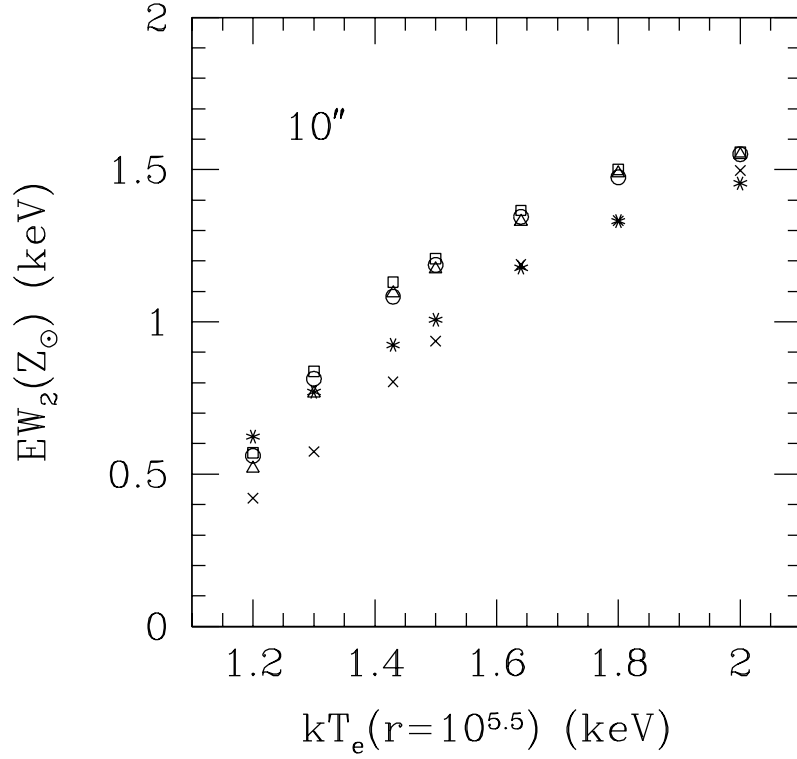
Fig. 4.— Variation of the equivalent width EW_2 of He-like iron line emission from the external medium ($\lesssim 10''$) as a function of the assumed external electron temperature $kT_e(r = 10^{5.5})$. Stars, crosses, squares, circles, and triangles correspond to the results for models A, B, C, D, E, respectively. Note that EW_2 shows a large variation with $kT_e(r = 10^{5.5})$ and modest variations among the five models.
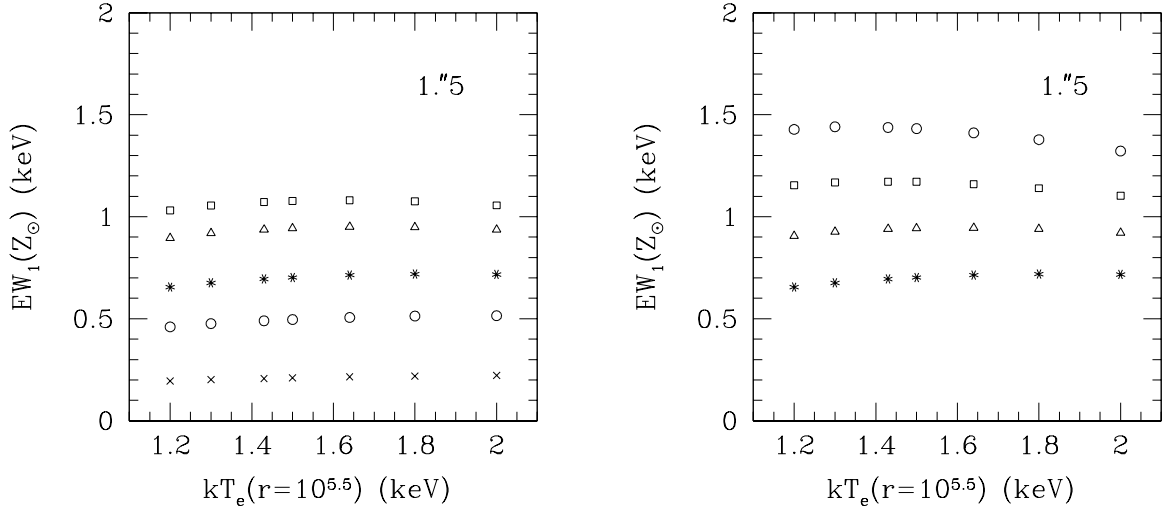
Fig. 5.— (a) Equivalent width of He-like iron line emission within 1.″5 of Sgr A* (EW_1) as a function of $kT_e(r = 10^{5.5})$ for different choices of the density power law index p of the RIAF (see eq. (1)). The external medium is described by model A. The five sets of results correspond to p=0.5 (squares), 0.75 (triangles), ∼1.13 (Yuan's model, stars), 1.25 (circles) and 1.5 (crosses). The models with p=1.25 and 1.5 are ruled out by radio polarization observations since these models predict a large gas density near the black hole. (b) Equivalent width of He-like iron line emission within 1.″5 of Sgr A* (EW_1) as a function of $kT_e(r = 10^{5.5})$ for four choices of the temperature profile in the RIAF. The external medium is described by model A. Stars correspond to Yuan et al's (2003) temperature profile. Triangles, squares and circles correspond to powerlaw temperature profiles with $q = 0.75,\ 0.5,\ 0.25$, respectively.

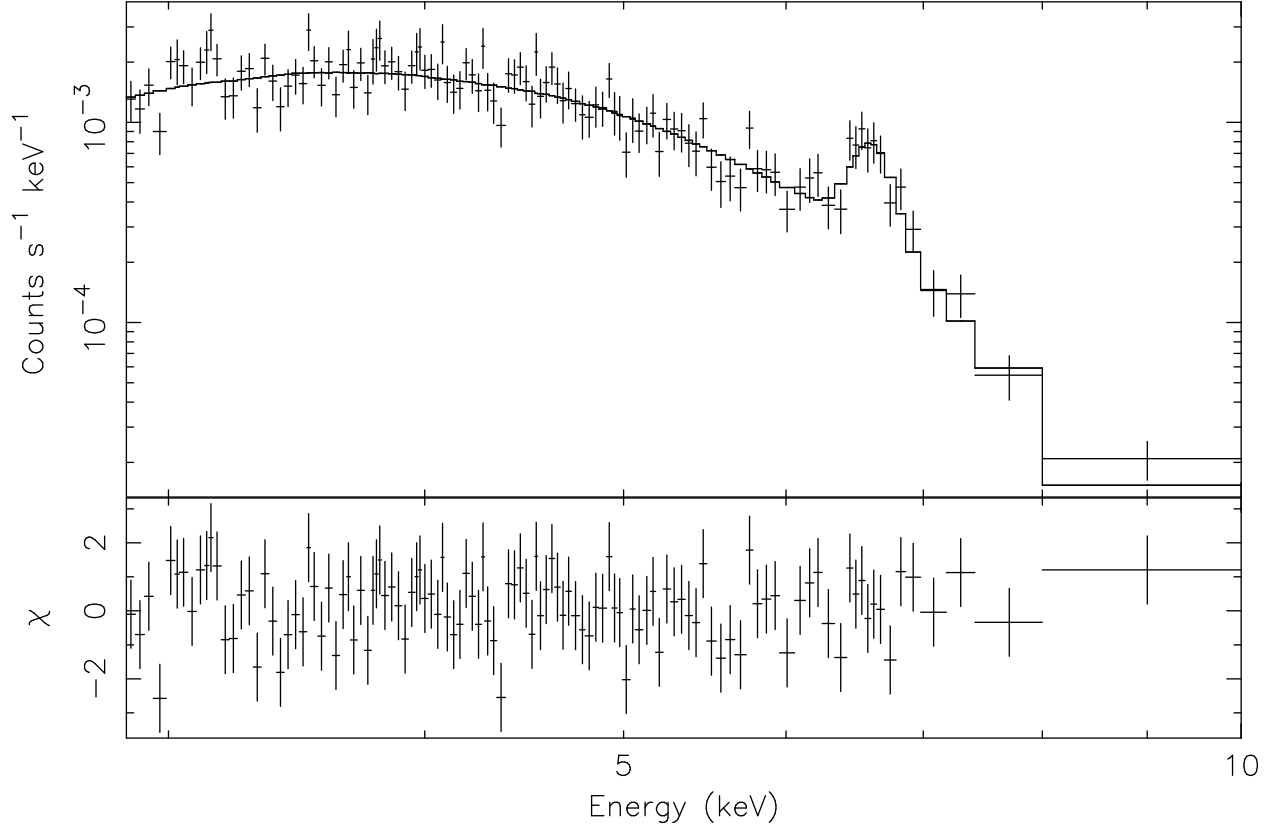Fig. 6.— Chandra spectrum of Sgr A* with the best-fit absorbed, dust-corrected, thermal bremsstrahlung plus Gaussian-line model (*solid line*). The lower panel shows the fit residuals in units of the standard deviation of the data.
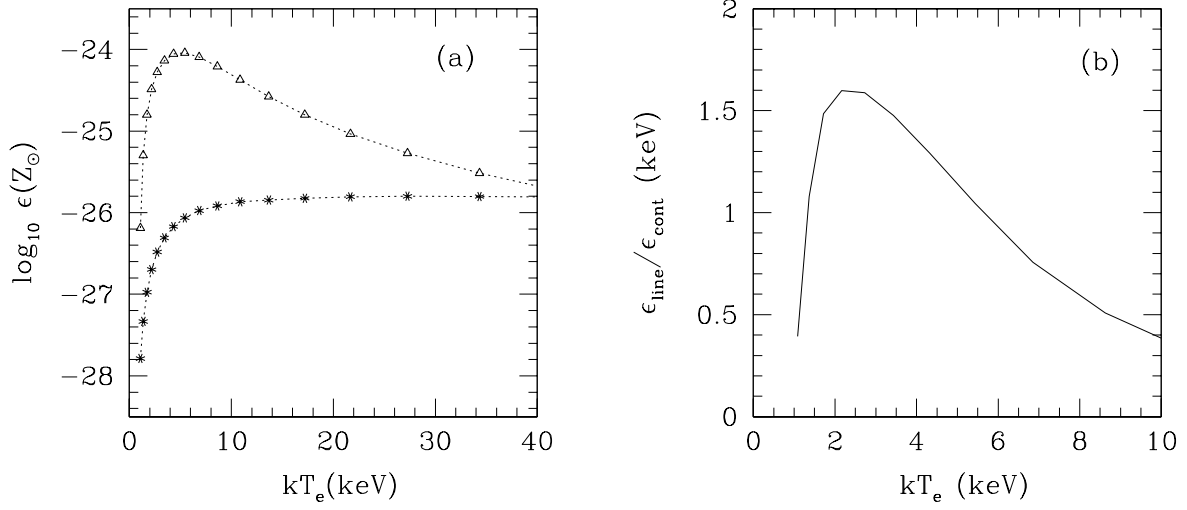
Fig. 7.— (a) Emissivity of He-like iron line (triangles) and 6.7 keV continuum (stars) for solar metallicity, calculated with the APEC code . The line emissivity $\epsilon_{\mathrm{line}}(Z_\odot)$ is in units of ergs cm^3 s^{-1}, while the continuum emissivity $\epsilon_{\mathrm{cont}}(Z_\odot)$ is in units of ergs cm^3 s^{-1} (9.9eV)$^{-1}$. (b) The ratio (in units of eV) of the line and continuum emissivities, i.e., the equivalent width of the line, as a function of electron temperature.